JOURNAL OF AIRCRAFT
Vol. 31, No. 4, July–Aug. 1994

Locally Interactive Laminar Separation Bubble Model

Paolo Dini*
Carleton College, Northfield, Minnesota 55057
and
Mark D. Maughmer†
Pennsylvania State University, University Park, Pennsylvania 16802

A semi-empirical laminar separation bubble model has been developed and incorporated into an airfoil design and analysis program. The generality and efficiency of this model have been achieved by approximating the local viscous/inviscid interaction, the transition location, and the turbulent reattachment process within the framework of an integral boundary-layer method. In particular, the whole bubble flowfield is found to depend on two empirically derived dimensionless parameters and on the transition location as calculated using linear stability theory. Comparisons of the predicted aerodynamic and boundary-layer characteristics with experimental measurements for several airfoils show excellent and consistent agreement for Reynolds numbers from 2×10^6 down to 1×10^5.

Nomenclature

A_1 = amplitude of turbulent H_{32} distribution upstream of reattachment
A_2 = amplitude of turbulent H_{32} distribution downstream of reattachment
b = width of separated shear layer
C_D = dissipation coefficient
C_p = pressure coefficient
c = airfoil chord
c_d = section drag coefficient
c_f = skin-friction coefficient
c_l = section lift coefficient
c_T = turbulent shear stress coefficient
DU = edge-velocity decrease as $l_1 \rightarrow \infty$
G = amplitude of Coles's wake function in Green's profiles
H_{12} = boundary-layer shape factor, δ_1/δ_2
H_{32} = boundary-layer shape factor, δ_3/δ_2
h = height of the bottom of separated shear layer on airfoil surface
l_1 = laminar length of the bubble
l_2 = turbulent length of the bubble
n_{crit} = value of the linear stability theory amplification factor at transition
P = pressure gradient parameter
R = chord Reynolds number, $U_\infty c/\nu$
R_{δ_2} = momentum thickness Reynolds number, $U\delta_2/\nu$
s = streamwise coordinate from the stagnation point
U = velocity at the edge of the boundary layer/inviscid velocity
U_∞ = freestream velocity
x = distance along airfoil chord
y = normal distance from the surface
α = angle of attack relative to the chord line
γ = separation angle
δ = boundary-layer thickness
δ_1 = boundary-layer displacement thickness
δ_2 = boundary-layer momentum thickness
δ_3 = boundary-layer kinetic energy thickness
θ = spreading angle of turbulent shear layer
ν = kinematic viscosity of air

Subscripts
$\mathcal{R}$ = turbulent reattachment point
$\mathcal{S}$ = laminar separation point
$\mathcal{T}$ = transition point

Received Dec. 9, 1992; revision received June 24, 1993; accepted for publication June 24, 1993.

*Visiting Assistant Professor, Department of Physics and Astronomy; Graduate Student, Department of Aerospace Engineering, Pennsylvania State University, University Park, PA. Member AIAA.

†Associate Professor, Department of Aerospace Engineering. Senior Member AIAA.

Introduction

AT chord Reynolds numbers of less than a million, the aerodynamics of airfoils are strongly influenced by the presence of laminar (transitional) separation bubbles. Examples of applications having airfoils which operate at such Reynolds numbers include sailplanes, wind-turbine blades, unmanned air vehicles (UAVs), high-altitude weather monitoring platforms, and compressor blades. As the Reynolds number decreases, the laminar boundary layer becomes progressively more stable causing transition to move downstream along the wing. If transition moves downstream of the minimum pressure point, the laminar boundary layer may separate causing transition to occur in the separated shear layer. The turbulent shear layer can then reattach such that a small pocket of recirculating fluid remains trapped next to the surface and is carried along by the wing. The maximum thickness of this "separation bubble" varies approximately from $0.001c$ at Reynolds numbers on the order of 2×10^6 to $0.01c$ at $R = 1 \times 10^5$. The boundary-layer assumptions apply to thin flows in which the variation of properties in the streamwise direction is much slower than in the cross-stream direction and the cross-stream momentum equation is negligible. The parabolic character of the governing equations that these assumptions imply corresponds to a unidirectional flow and precludes the description of a separated flow as a boundary-layer flow. Because the ratio of the thickness to the length of a weakly interacting laminar separation bubble is always approximately 0.05, however, its locally elliptic nature is well modeled by imposing an independently obtained boundary condition *downstream* of the bubble, while still calculating the flow development *inside* the bubble by means of a boundary-layer method.

If the bubble does not reattach, it is termed "burst." In the first 40 yr after bubbles were first observed by Melville Jones in 1933,[1] the emphasis in the study of bubbles was placed on the very short bubbles that form near the leading edge of airfoils at high angles of attack and relatively high Reynolds numbers. In fact, the bursting of such bubbles is often the

cause of the abrupt stall behavior of some wings. In the last 20 yr, interest in the development of UAVs has shifted the range of Reynolds numbers studied to values below 1×10^6. In this range, bubbles form also at low lift coefficients near the midchord. Although they may be as much as $0.3c$ in length, as long as they reattach they are still called "short" or "weakly interacting." This study was inspired by the observation that short bubbles modify the inviscid velocity distribution only locally: it should be possible, therefore, to model them through local parameters as opposed to resorting to less efficient, global interaction methods.

Of the many characteristics and effects of a separation bubble, the increase in profile drag that results from its presence is generally the most difficult to determine. The increase in drag that accompanies separation bubbles is primarily due to the rapid increase in momentum thickness that occurs in a bubble compared to the much smaller growth that occurs with a natural transition from a laminar to a turbulent boundary layer. As a consequence, when a separation bubble is the mechanism of transition, methods that assume that transition occurs at the laminar separation point, and use the boundary-layer properties at that point as the initial conditions for the turbulent boundary-layer calculations, usually underpredict the drag. Thus, to successfully determine the increase in drag on an airfoil due to separation bubbles, it is necessary to model accurately the development of the boundary layer through the bubble.

While a number of empirically based separation bubble models have been introduced in the past, some of which are detailed in Ref. 2, the majority of these assume that the bubble development is fully predictable from upstream conditions. More recently, better predictions have been made possible using viscous/inviscid interaction approaches such as those described in Refs. 3–8. By such means, the influence of the bubble on the entire velocity distribution over the airfoil is accounted for globally by iterating between the inviscid flow and boundary-layer solutions. While not of much concern in predicting the aerodynamic characteristics of a single airfoil, the amount of computational time required for such boundary-layer iteration methods becomes consequential in the case of airfoil design, for which the number of analysis cases required can become very large.

One way of accounting for laminar separation bubbles in airfoil design is the bubble analog used in the design and analysis program of Eppler and Somers.[9,10] In this method, the designer is warned about the presence of separation bubbles which might unacceptably increase the drag over that which is predicted assuming that transition occurs at laminar separation. Although this approach has proven very useful in designing airfoils for Reynolds numbers greater than 5×10^5, below this value the drag caused by a bubble can be as much or more as that caused by the rest of the airfoil. In such cases, it would be advantageous to be able to predict the actual impact of separation bubbles on section properties, provided that this can be done without significantly increasing computational requirements. Toward this end, a locally interactive separation bubble model has been developed and incorporated into the Eppler and Somers program.[11] Although unable to account for strong interactions such as the large reduction in suction peak sometimes caused by leading-edge bubbles, it is able to predict the increase in drag and the local alteration of the airfoil inviscid pressure distribution that is caused by bubbles occurring in the operational range of most interest.

To determine fully the behavior and influence of a laminar separation bubble, it is necessary to predict accurately the shear-layer development in the regions of the bubble indicated in Fig. 1. The formation of a bubble is initiated at point $\mathcal{S}$, shown in the figure, by the laminar boundary layer separating from the airfoil surface. Using integral boundary-layer methods this point can be accurately determined. Once separated, the free shear-layer development must be tracked and the

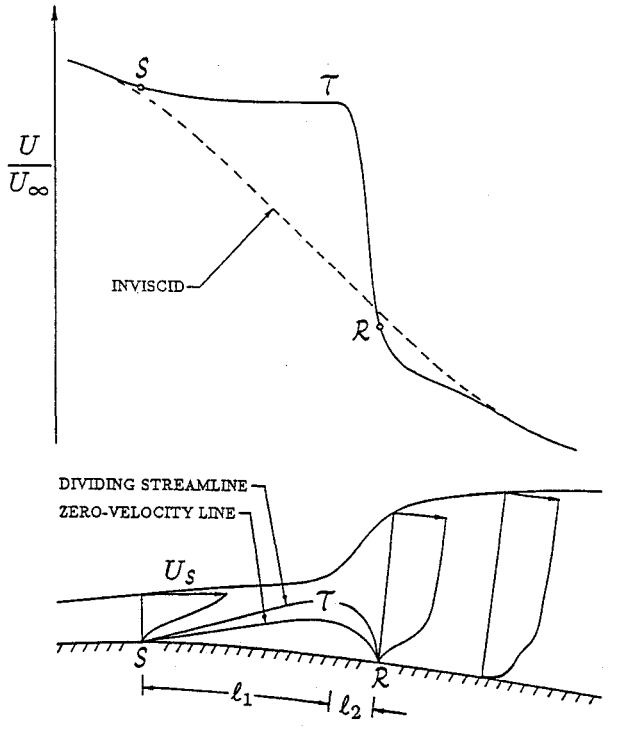

Fig. 1 Sectional view of a two-dimensional short laminar separation bubble and its influence on the velocity distribution over an airfoil.

transition from laminar to turbulent flow, which occurs near the point $\mathcal{T}$, predicted. As shown in the figure, the separation bubble causes a plateau to form in the edge-velocity distribution between the points corresponding to laminar separation and the end of the transition region. From this point, the efficient cross-stream transfer of momentum of the turbulent Reynolds stresses entrains the momentum of the outer flow, of which there is no shortage, and brings it next to the wall. This allows the separated shear layer to reattach at point $\mathcal{R}$, recovering the inviscid pressure over a very short distance. The loss of outer-flow momentum results, by definition, in a rapid growth of boundary-layer thickness in the turbulent part of the bubble. In terms of the variables of the model, this loss of outer flow momentum that is necessary to achieve reattachment results in a rapid growth in momentum thickness, which is ultimately responsible for the increase in drag caused by the bubble. As an additional pressure recovery always occurs downstream of a reattachment point, the velocity distribution corresponding to the highly nonequilibrium, relaxing boundary layer downstream of reattachment "undershoots" the inviscid distribution. Eventually, the turbulent boundary layer reaches its fully developed state and the undershoot region merges smoothly from below with the inviscid velocity distribution. Clearly it is possible, especially at low Reynolds numbers, that the turbulent boundary layer does not reach equilibrium before the trailing edge of the airfoil.

The qualitative description of the kinematics and dynamics of the bubble given above cannot be readily translated into a direct boundary-layer analysis because of the singularity that develops at laminar separation. Rather than resorting to a fully inverse, strongly interacting method, the local character of the short bubble interaction points to a solution method that falls between the direct and the inverse procedures. The bubble as a whole appears to be "driven" in the direct mode by the characteristics of the inviscid velocity distribution in its vicinity, whereas the flow details inside it are determined by the viscous solution. Given the input conditions at the "boundaries" of the bubble (i.e., at the separation and reattachment points), the model must be able to produce the viscous solution within these boundaries. Through judicious dimensionless groupings of the relevant boundary conditions, the entire bubble flowfield is shown to depend on two em-

pirically derived dimensionless parameters. A third parameter obtained independently is the linear stability theory amplification factor that determines the length of the laminar part of the bubble. The identification of the parameters controlling the bubble has made possible the development of five empirical functions (hence, the attribute "semi-empirical" that this model bears) that complement the governing differential laws and allow the determination of the complete bubble flowfield.

Local Parameters

For at least three decades it has been known that the characteristics of laminar separation bubbles depend on chord Reynolds number, momentum thickness at laminar separation, and the average inviscid velocity gradient along the bubble. Gaster,[12] in fact, was able to express the boundary between bubbles that reattach and bubbles that burst in terms of two dimensionless parameters obtained by conveniently grouping these three variables. The bursting locus that results is expressed as a curve defined by the momentum-thickness Reynolds number at laminar separation

$$(R_{\delta_2})_{\mathcal{S}} = \frac{U_{\mathcal{S}}(\delta_2)_{\mathcal{S}}}{\nu} = R\frac{U_{\mathcal{S}}}{U_\infty}\frac{(\delta_2)_{\mathcal{S}}}{c} \tag{1}$$

and Gaster's pressure gradient parameter

$$P = \frac{(\delta_2)^2_{\mathcal{S}}}{\nu}\frac{\Delta U}{\Delta s} = R\left[\frac{(\delta_2)_{\mathcal{S}}}{c}\right]^2\frac{\Delta(U/U_\infty)}{\Delta(s/c)} \tag{2}$$

Another example of how these parameters can be used to model the bubble is provided by Wortmann,[13] who found that available measurements of the angle between the dividing streamline at laminar separation and the surface are well correlated by the expression

$$\tan\gamma = -[64P/(R_{\delta_2})_{\mathcal{S}}] \tag{3}$$

This expression is used in the present model. It was found better than a similar expression proposed by van Ingen and Boermans[14] in which the factor $-64P$ is replaced by a constant with the value of 17.5.

A third example of the use of the parameters characterizing the bubble is given in Ref. 11 where it is shown that the amount of pressure recovered in the laminar part of the bubble is well represented as a function of P. This parameter embodies some of the boundary conditions alluded to above: $(\delta_2)_{\mathcal{S}}$ and, through the inviscid gradient, the pressure at reattachment. As discussed in Refs. 10, 15, and 16, the convenience of choosing boundary or initial conditions as reference quantities lies in the fact that this removes the explicit dependence of the solution on them. The whole solution is then expressible in terms of variables whose *units* are the boundary or initial conditions themselves.

By fitting the data of Refs. 17–20, as shown in Fig. 2, the pressure recovered in the laminar part of the bubble can be expressed as

$$DU = -(0.003/P) \tag{4}$$

DU is the dimensionless fraction of $U_{\mathcal{S}}$ that is recovered between $\mathcal{S}$ and $\mathcal{T}$. This particular correlation can be justified by the proportionality of P to $(\delta_2)_{\mathcal{S}}$. Since δ_2 measures momentum *lost*, a small value of $(\delta_2)_{\mathcal{S}}$ means that a significant amount of momentum is still present in the boundary layer at separation. It is therefore not surprising that a greater amount of pressure recovery should be possible. Alternatively, this correlation can be thought of as embodying the inviscid displacement thickness effect. This can be seen most easily by comparing leading-edge bubbles with midchord bubbles. Leading-edge bubbles always have a very small value of

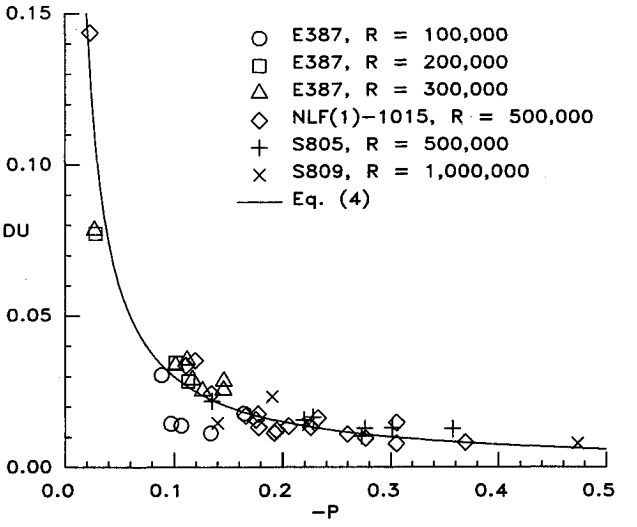

Fig. 2 Pressure recovery in the laminar part of the bubble as a function of Gaster's pressure gradient parameter.[12]

$(\delta_2)_{\mathcal{S}}$, which leads to a large value of DU. As a consequence, a significant amount of pressure is recovered in the laminar part of a leading-edge bubble, which is consistent with the small effect such thin bubbles have on the inviscid outer flow. Midchord bubbles, by contrast, tend to be much thicker and to have much greater values for $(\delta_2)_{\mathcal{S}}$, in comparison. The corresponding displacement thickness distribution is such that it provides a sizable obstacle to the inviscid flow, thereby causing the observed plateau in pressure and small value of DU. By capturing the correct behavior of the pressure distribution by means of Eq. (4), the necessity to iterate on the displacement thickness to arrive at the correct bubble solution is bypassed. Similarly, the expression for the dividing streamline, Eq. (3), by relying on the same parameter is able to capture the same effect.

The edge-velocity distribution in the laminar part of the bubble, then, is found by generalizing an exponential function proposed by van Ingen[14]

$$\frac{U}{U_{\mathcal{S}}} = 1 - DU\left\{1 - \exp\left[\frac{1}{DU}\frac{U'_{\mathcal{S}}}{U_{\mathcal{S}}}(s - s_{\mathcal{S}})\right]\right\} \tag{5}$$

The value of $DU = 0.022$ used by van Ingen falls in the middle of the variation shown in Fig. 2 for midchord bubbles, whereas it is inadequate for leading-edge bubbles. Equation (5) incorporates the remaining boundary conditions to be satisfied, $U_{\mathcal{S}}$ and $U'_{\mathcal{S}}$, the inviscid velocity gradient at laminar separation.

When the independently obtained linear stability theory amplification factor n reaches the value of 11, transition to turbulent flow is assumed.[21] Based on the laminar solution at the transition point, three additional functions can be defined that allow the integration of the solution to the reattachment point and beyond to a smooth merging with the inviscid distribution where calculations in the direct mode are resumed.

Laminar Part of the Bubble

The present analysis uses the same laminar boundary-layer method that is employed in the Eppler and Somers program, where the inviscid velocity distribution drives the laminar boundary-layer development according to the integral momentum and energy equations[22]

$$\frac{d\delta_2}{ds} = \frac{c_f}{2} - (H_{12} + 2)\frac{\delta_2}{U}\frac{dU}{ds} \tag{6}$$

$$\frac{d\delta_3}{ds} C_D - 3\frac{\delta_3}{U}\frac{dU}{ds} \tag{7}$$

As the boundary-layer method uses the Falkner-Skan profiles upstream of the bubble, laminar separation is predicted when the shape factor reaches the corresponding value for these profiles

$$H_{32} = 1.515095 \tag{8}$$

Starting immediately downstream of the laminar separation point, the shear layer development is found by integrating Eqs. (6) and (7) in the direct mode with the velocity distribution given by Eq. (5). Since the correct value of P is not known beforehand, an initial estimate is used and the whole bubble solution iterated until the value of P used equals the value actually driving the bubble. This is equivalent to a standard shooting method used to solve boundary-value problems.

Equations (6) and (7) can be complemented with closure correlations derived from the reversed Falkner-Skan, or Stewartson,[23] velocity profiles. As discussed in Ref. 24, however, experimental measurements indicate that the Stewartson profiles do not reflect the actual velocity distribution in the laminar part of the bubble; rather, the measured flowfield is matched better by the two-parameter profile family originally developed by Green[25] for a turbulent shear layer forming a free stagnation point downstream of a base. These profiles are defined by the following function:

$$\frac{u}{U} = \begin{cases} 1 - 2G, & 0 < y \le h \\ 1 - G\left[1 + \cos\left(\pi \dfrac{y - h}{b}\right)\right], & h < y \le h + b \end{cases} \tag{9}$$

Thus, (h/b) is the ratio of the distance between the bottom of the shear layer and the wall to the width of the shear layer. G is the amplitude of Coles's wake function. Since there is slip at the wall, these profiles cannot be utilized to develop a relationship for c_f. This shortcoming can be remedied by the skin-friction correlation developed in Ref. 26 in which a finite-difference calculation of the bubble flowfield has led to very similar profiles. The skin-friction coefficient obtained from this correlation, which is smaller in absolute value than that from the Falkner-Skan profiles, is given by

$$R_{\delta_2}\frac{c_f}{2} = \begin{cases} -0.07 + 0.0727\dfrac{(5.5 - H_{12})^3}{H_{12} + 1}, & H_{12} < 5.5 \\ -0.07 + 0.015\left(1 - \dfrac{1}{H_{12} - 4.5}\right)^2, & H_{12} > 5.5 \end{cases} \tag{10}$$

The use of such geometrically simple yet two-parameter profiles poses a significant challenge in that their shape is not automatically determined by the dynamics of the boundary layer, as in the Falkner-Skan case, but relies on a detailed knowledge of the flow geometry in the laminar part of the bubble. Such flow geometry must still be compatible with the basic conservation laws of mass, momentum, and energy. The measurements of Ref. 24 indicate that the amount of backflow is small (less than 15% of the boundary-layer edge velocity), and this is confirmed by the present model. Based on flow visualization and an analytical solution of the Navier-Stokes equations near the laminar separation point discussed in Ref. 27, the dividing streamline is assumed to be a straight line oriented at the separation angle relative to the surface. After careful study, it was concluded that airfoil curvature has little or no effect on the so-called short or weakly interacting bubble, even when it forms near the leading edge. Remaining entirely within the approximations of conventional boundary-layer theory, therefore, there is sufficient information to define correctly the details of the flowfield in the laminar part of the bubble.

The simple geometrical definition of the Green profiles, Eq. (9), allows δ_2/b and H_{32} to be expressed explicitly in terms of the two parameters h/b and G. These relationships can be used as constraints to solve for b and G. By forcing the net flow between the wall and the dividing streamline to equal zero, a third independent equation is obtained from which h can be determined. The boundary-layer thickness at laminar separation and $h = 0$ are used as initial estimates for b and h in the definition of H_{32} for the Green profiles, where H_{32} is determined by integration of the momentum and energy integral equations. G can thus be calculated using the quadratic formula

$$G = -\frac{(1.5 + 4h/b)(H_{32} - 3)}{2(2.5 + 8h/b)} + \frac{\sqrt{(1.5 + 4h/b)^2(H_{32} - 3)^2 + 4(2.5 + 8h/b)(1 + 2h/b)(H_{32} - 2)}}{2(2.5 + 8h/b)} \tag{11}$$

Only the positive root corresponds to physical solutions. This value of G is then substituted with h and b into the condition requiring zero net mass flow between the wall and the dividing streamline y_D

$$\frac{y_D}{b} - G\left[\frac{y_D + h}{b} + \frac{1}{\pi}\sin\left(\pi\frac{y_D - h}{b}\right)\right] = 0 \tag{12}$$

This expression is obtained by integrating Eq. (9) between the wall and y_D. The value of h is iterated upon, updating G with Eq. (11) but leaving b fixed, until Eq. (12) is satisfied. Upon convergence, the new values of G and h are utilized together with the old value of b in the definition for δ_2

$$(\delta_2/b) = G[1 - 1.5G + 2(h/b)(1 - 2G)] \tag{13}$$

The value of b is now iterated upon, updating G with Eq. (11) but leaving h fixed, until this expression is satisfied also. The whole process is repeated until both Eqs. (12) and (13) are satisfied simultaneously. Interval halving is used instead of Newton's method because multiple values of h can satisfy this system. Upon convergence, H_{12} and C_D are obtained from the correlations for the Green profiles

$$H_{12} = \frac{3(1 - G) - H_{32}}{(1 - G)(1 - 2G)} \tag{14}$$

$$R_{\delta_2}C_D = \frac{\pi^2 G^3}{2} \times \left[1 - \frac{3}{2}G - \frac{(4 - 5G)(1 - G) - (2 - 3G)H_{32}}{4(1 - G) - 2H_{32}}\right] \tag{15}$$

Using the Green profiles in this particular way, the flowfield in the laminar part of the bubble is calculated in a manner that is consistent with conservation of mass, momentum, and energy.

Transition

The transition location, assumed to occur at a point, is found by means of a linear stability analysis of the Falkner-Skan profiles upstream of separation and of the Green profiles downstream of separation. In order to keep the computational requirements low, the data base look-up method developed by Stock and Degenhart[28] has been extended to separated boundary layers. This method is discussed in depth in Ref. 21 where it is shown that, if used in conjunction with the

Green profiles, it is much more accurate than the so-called envelope methods that are based solely on the Falkner-Skan profiles. This greater accuracy is attributable to the use of the Green profiles as well as to errors arising from the assumption of local similarity inherent in the envelope methods of Refs. 3 and 29. While this assumption is permissible for attached boundary layers, in fact, it leads to significant errors downstream of laminar separation due to the steep growth of H_{12}. Following the amplification of each frequency, as is done in Ref. 21, correctly captures the effects of variations in both local Reynolds number and shape factor. In the results to be discussed below, $n_{crit} = 11$ is used for all the predictions that are considered. This particular value best matches the stability characteristics of the Green profiles with observed transition locations.

Turbulent Part of the Bubble

The calculation of the turbulent part of the bubble relies on the assumption that reattachment will occur. An independent bursting criterion has not been devised, nor have existing ones been tested. The reason is that bursting occurs either at very low Reynolds numbers or when the mean inviscid pressure gradient becomes too steep downstream of a suction peak, and both conditions represent extremes that lie outside the capabilities of the simple approach taken with the present model. This is not so much because of a failure of the bubble model itself but, rather, because at such extremes the onset of strong global viscous/inviscid interaction causes the inviscid pressure distribution that drives the model to be modified too much. Limiting the generality of the mathematical model strictly to a weak-interaction algorithm has forced a deeper understanding of the bubble dynamics than would otherwise have been necessary and has led to drag predictions more accurate than any of the existing interactive methods.

Unlike in the laminar part, it is more convenient in the turbulent part of the bubble to approximate the distribution of H_{32} than that of the edge velocity. In fact, given that the value as well as the slope of the H_{32} distribution is always known at the reattachment point, a general function has been developed which allows the solution of the turbulent part of the bubble in the inverse mode. The distribution of H_{32} is specified in normalized form as

$$\bar{H}_{32}(\bar{x}) = \sin(\pi/\bar{x}) \tag{16}$$

where

$$\bar{H}_{32} = \frac{H_{32} - (H_{32})_{\mathcal{R}}}{A_i[(H_{32})_{\mathcal{T}} - (H_{32})_{\mathcal{R}}]} - 1$$

$$\bar{x} = (\bar{s} - \bar{x}_0)\sigma + \bar{x}_0 \tag{17}$$

$$\bar{x}_0 = \frac{\pi}{3\pi - \sin^{-1}(1/A_1 - 1)}$$

$$\sigma = \begin{cases} (s - s_{\mathcal{T}})/l_2, & s \le s_{\mathcal{R}} \\ [(s - s_{\mathcal{T}})/l_2 - 1]\sqrt{(A_1/A_2)} + 1, & s > s_{\mathcal{R}} \end{cases}$$

The factor $\sqrt{A_1/A_2}$ ensures continuity in the curvature of $H_{32}(s)$ at the reattachment point, and the subscript "i = 1, 2" refers to the amplitude of the H_{32} function upstream and downstream of reattachment, respectively. This function is shown in normalized form in Fig. 3.

The inverse boundary-layer formulation employed here, where the distribution of shape factor is specified,[10] is especially convenient and powerful since it allows complete control of the boundary-layer behavior in an otherwise extremely sensitive region while, at the same time, relying on an intrinsically general function. Such effectiveness, however, comes at a price. While specification of the pressure recovery distribution, if the correct one were indeed known in general, would automatically drive the boundary layer to reattach at the correct location, the turbulent length of the bubble, l_2 in Eq. (17), is not known a priori and must be found by independent means. The local flowfield is driven by a turbulent momentum-transfer mechanism whereby the outer momentum brought toward the wall accelerates the near-stagnant reverse flow until reattachment is achieved. Reattachment, therefore, becomes dependent on the efficiency of this mechanism. In geometrical terms, the reattachment location becomes dependent on the spreading angle of the turbulent shear layer and on the initial distance of the shear layer from the wall.

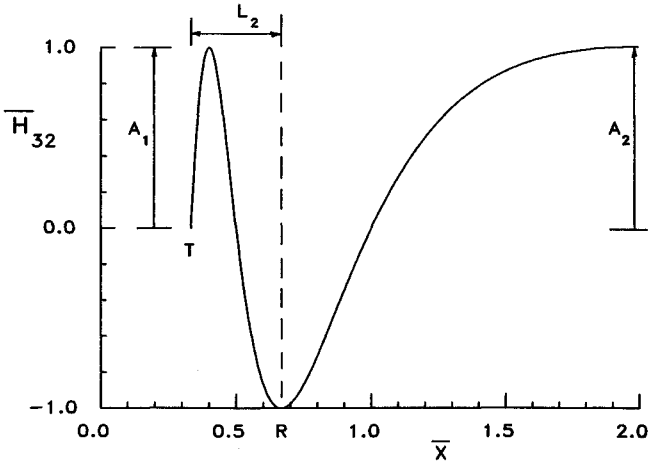

Fig. 3 Normalized shape factor turbulent recovery function.

Following Eppler,[10] the distribution of H_{32} described above is input into the momentum and energy integral equations expressed in the inverse mode

$$\frac{dU}{ds} = \left[(c_f/2)H_{32} - C_D + \delta_2 \frac{dH_{32}}{ds}\right] \frac{U}{\delta_2 H_{32}(H_{12} - 1)} \tag{18}$$

$$\frac{d\delta_2}{ds} = \left[-\frac{3(c_f/2)H_{32}}{H_{12} + 2} + C_D - \delta_2 \frac{dH_{32}}{ds}\right] \frac{H_{12} + 2}{H_{32}(H_{12} - 1)} \tag{19}$$

The closure correlations from Ref. 3 are utilized, where use is made of an additional equation for the rate of change of the turbulent shear stress and the shape factor correlation is derived from the analytical profiles of Swafford,[30] even though these profiles could be improved for values of $H_{12} > 6$. In the present method, this correlation needs to be expressed in the form $H_{12}(H_{32})$. Since the correlation presented in Ref. 3 is expressed as $H_{32}(H_{12})$ and cannot be inverted, a close approximation has been developed. Defining first

$$H_{32_0} = 1.505 + \frac{4}{R_{\delta_2}} \qquad H_{12_0} = 3 + \frac{400}{R_{\delta_2}}$$

$$c_1 = 0.081(R_{\delta_2} - 300)^{0.1}$$

$$c_2 = 0.0158(R_{\delta_2} - 300)^{0.08} \tag{20}$$

$$c_3 = 1.06 + \frac{3000}{(R_{\delta_2} + 600)^{1.5}}$$

H_{12} is obtained from

$$H_{12} = \begin{cases} \dfrac{H_{12_0}}{1 + [H_{32} - H_{32_0}/c_1]^{1/1.27}}, & c_f > 0 \\ H_{12_0} + [H_{32} - H_{32_0}/c_2]^{1/c_3}, & c_f < 0 \end{cases} \tag{21}$$

This expression, as the original, is valid for $R_{\delta_2} > 400$. The skin-friction law of Swafford[30] closes the system.

Three Empirical Functions

Spreading Rate

Measurements by Birch and Eggers[31] indicate that the spreading rate of turbulent shear layers developing in zero pressure gradient is well correlated to the velocity ratio between the two streams, defined as

$$\lambda = [(u_1 - u_2)/(u_1 + u_2)] \tag{22}$$

where u_1 is the velocity above a splitter plate and u_2 is below. The experiments were performed for values of λ ranging from 0 to 1, corresponding to $u_2 = u_1$ and $u_2 = 0$, respectively. For these cases, the simple function applies

$$(\tan\theta/\tan\theta_0) = \lambda \tag{23}$$

Here, $\tan\theta_0$ is a reference value corresponding to the spreading rate when $\lambda = 1$ and is equal to 0.11. In order to obtain the spreading rate of the shear layer inside the bubble, Eq. (23) is extrapolated to the case of negative u_2, which, for the bubble, corresponds to values of λ slightly larger than 1. Since the formulation of the laminar part includes an estimate for the amount of backflow at transition, this can be used directly to calculate λ. In terms of the variables used here, Eq. (23) becomes

$$\tan\theta = 0.11[G/(1 - G)]_{\mathcal{T}} \tag{24}$$

The angle θ is used to calculate the length of the turbulent part of the bubble using the simple expression

$$l_2 = (h_{\mathcal{T}}/\tan\theta) \tag{25}$$

where $h_{\mathcal{T}}$ is the height of the bottom of the laminar shear layer at transition. Figure 4 shows this angle together with the geometrical structure of the whole bubble flowfield. While in the laminar part the displacement thickness effect was captured through Eqs. (3) and (4), in the turbulent part it is captured by Eqs. (16) and (25), which determine how quickly δ_1 decreases.

The data of Ref. 31 are all taken in shear layers developing in zero pressure gradient, so that their validity in the turbulent part of the bubble, where the pressure varies very rapidly, could be doubted. Making recourse to the strongly interacting nature of the flow, however, the above objection can be dispelled. Specifically, this shear layer is not developing inside a duct with diverging walls, where the pressure gradient is imposed as a boundary condition of the inviscid flow. In the bubble, the amount of pressure recovered is strictly a function of the intensity of the turbulence, or the momentum transfer across the shear layer. Therefore, treating the reattaching turbulent shear layer in the bubble as a shear layer in zero pressure gradient with varying velocity ratios, and the rise in pressure a by-product with negligible feedback, seems to be a reasonable approximation. Rather than directly influencing the location of turbulent reattachment, in fact, the inviscid gradient imposed over the whole bubble flowfield only affects the pressure distribution in the laminar part through the function $DU(P)$, Eq. (4).

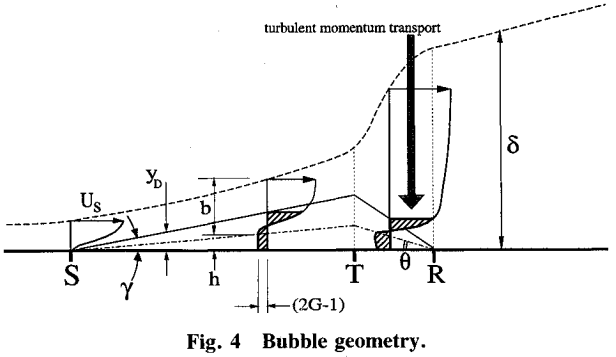

Fig. 4 Bubble geometry.

Initial Value for c_T

The second most important variable of the bubble model is the value of the dissipation coefficient used in the turbulent part of the bubble. The dissipation coefficient is the integral of the turbulent shear stress across the boundary layer. In an integral method, therefore, it is this variable that supplies information to the momentum and energy balances about the importance of the effects of the turbulence. A large value for C_D implies a high intensity of turbulence and, not surprisingly, causes a more rapid growth of the momentum thickness and a steeper pressure recovery. Since most of the drag caused by a bubble arises from its turbulent part, it is clear that for an accurate drag prediction both the length of the turbulent part of the bubble and the value of C_D must be approximated very closely.

In the nonequilibrium turbulent boundary-layer method presented in Ref. 3 and adopted in the present bubble model, the dissipation coefficient is a function of c_T. The value of C_D obtained with this boundary-layer method is too low for the turbulent part of the bubble, and it was therefore approximately doubled in Ref. 11. In recent modifications to the ISES and XFOIL programs, Drela[26] also increased the value of this variable in the turbulent part of the bubble by increasing the initial value of c_T. In order to match measured pressure distributions better, Drela has correlated this parameter with the value of H_{12} at transition. Using this function within the present method has not led to very satisfactory drag predictions. By analogy with the spreading rate, rather, it is postulated that a better independent variable may be the velocity ratio λ such that

$$F_T = \lambda = [G/(1 - G)]_{\mathcal{T}} \tag{26}$$

F_T is the ratio of c_T to its equilibrium value, given by the local conditions of the boundary layer at transition. This function is consistent with the notion that a greater velocity difference should lead to more vigorous mixing of the streams.

Amplitude of H_{32}-Function

Having determined l_2, Eq. (16) is completely specified when values are assigned to A_i. The value for A_1 may be linked to the length of the transition region. In accordance with the H_{32}-distributions measured by Horton,[32] as well as more recently by Fitzgerald and Mueller,[24] A_1 is such that H_{32} grows steeply downstream of transition to a local maximum before dropping to the reattachment value. This is consistent with the initial thinning of the shear layer immediately downstream of transition caused by the turbulent transfer of momentum between the streams. The linear growth of turbulent shear layers soon thereafter brings the shape-factor value back down, toward reattachment. By matching measured drag and pressure distributions, the local maximum between $\mathcal{T}$ and $\mathcal{R}$ is never allowed to be smaller than 1.6 or greater than 3 and, otherwise, it is given by

$$(H_{32})_{\max} = 1.515095 + 2[(H_{32})_{\mathcal{T}} - 1.515095] \tag{27}$$

Downstream of $\mathcal{R}$, two distinct cases can arise:

1) If the pressure at $\mathcal{R}$ is higher, equal, or only slightly lower than the inviscid, an "undershoot" is allowed to form, in accordance with measurements, and the correct value of the amplitude of the $\sin(\pi/\bar{x})$ function downstream of $\mathcal{R}$, A_2, is found by enforcing smooth merging of the undershoot with the inviscid distribution.

2) If, on the other hand, the pressure at $\mathcal{R}$ is significantly lower than the inviscid at the same station, then normal

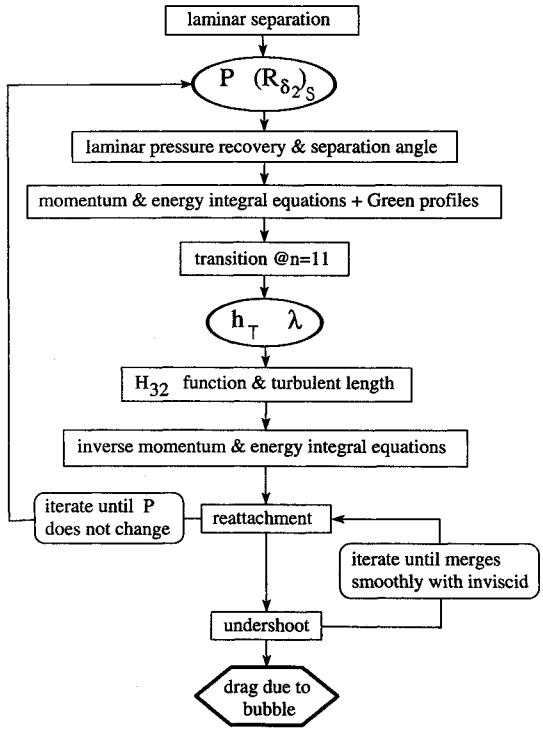

Fig. 5 Flow chart of computational scheme used to model laminar separation bubbles.

boundary-layer calculation in the direct mode is resumed upon the first crossing with the inviscid distribution.

The problem here is that different values of A_2 will work giving, however, rather different values of drag. Again using comparisons with drag data, a very small value of A_2 has been found to be best. This physically corresponds to a very vigorous turbulent boundary layer downstream of a thin bubble that achieves fully developed or near-equilibrium state very quickly, by producing a large momentum flux from the outer flow toward the wall. This effect is modelled mathematically as a large growth of δ_2 and, therefore, a relatively slow growth of H_{32} which is obtained with a small value of A_2.

The overall scheme for the bubble model calculation is shown schematically in Fig. 5.

Comparisons with Measurements

Although the present model can be used in a variety of viscous analysis methods for incompressible airfoil flows, it was developed with the purpose of using it with the airfoil design and analysis program of Eppler and Somers.[9] This program employs a conformal mapping method that allows for multipoint design by specifying different characteristics of the velocity distribution over different segments of the airfoil. The exact inviscid distribution thus obtainable is then analyzed by means of an integral boundary-layer method utilizing the momentum and energy integral equations. Although a displacement-thickness iteration can be prescribed for calculating the zero-lift angle of attack more accurately, assuming that the boundary layer and outer flows interact weakly yields very accurate drag polars for an extremely small computational cost. Near maximum lift, of course, the viscous/inviscid interaction is not weak, but the program utilizes an approximation to account for the effects of turbulent separation that has been used successfully on a large number of airfoils.

The accuracy of the laminar separation bubble model has been tested extensively by comparing its predictions to measurements of boundary-layer, pressure distribution, and aerodynamic characteristics for many different airfoils at different angles of attack and Reynolds numbers. Only a few representative predictions are included in this article due to space limitations.

Boundary-Layer Characteristics

Figures 6 and 7 show comparisons with pressure and boundary-layer measurements taken within the bubble flowfield[33,34] together with the corresponding inviscid, measured, and predicted pressure distributions. These predictions would probably benefit from an intermittency function to simulate the finite transition region typical of lower Reynolds number flows. The overall behavior of the pressure, momentum thickness, and shape factor is, nonetheless, captured very well. The step in the H_{12}-distribution at the laminar separation point is caused by the Goldstein singularity. Although a locally inverse procedure that eliminates this singular behavior has been developed, it is not used because this singularity has been found to have no discernible effect on the pressure or drag predictions. The n developments for 10 different frequencies are shown along the surface of the airfoil, plotted in units of percent chord above (or below, for the lower surface) corresponding y coordinates. In both cases, the theoretical coordinates have been used instead of the actual model coordinates. The inviscid velocity distribution is generated by means of the higher-order panel method employed in the Eppler and Somers program.[9] The inviscid pressure distribution of Fig. 6 is significantly different from that measured because of the large amount of aft-loading. While the bubble flowfield compares favorably, at this low Reynolds number the drag would probably be predicted more accurately by an interactive method employing the present bubble model.

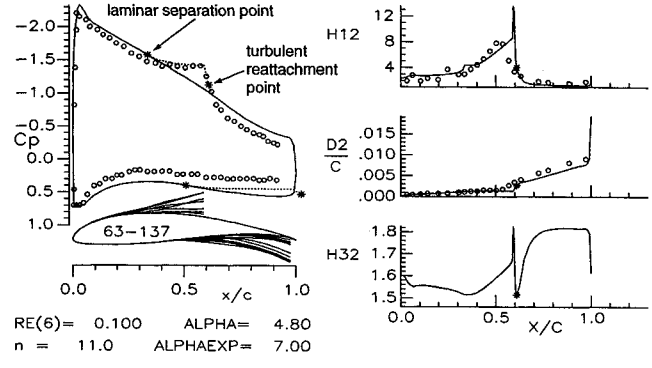

Fig. 6 Comparison of predicted and measured pressure distribution and boundary-layer development over the Wortmann FX 63-137 airfoil. Solid line: inviscid pressure distribution and predicted boundary-layer development; dotted line: bubble pressure distribution; circles: data from Ref. 33.

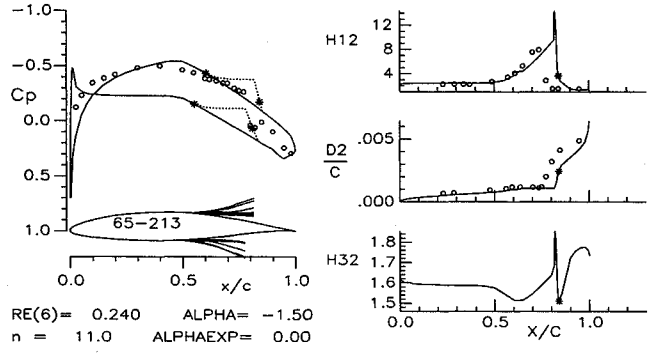

Fig. 7 Comparison of predicted and measured pressure distribution and boundary-layer development over the NACA 65-213 airfoil. Solid line: inviscid pressure distribution and predicted boundary-layer development; dotted line: bubble pressure distribution; circles: data from Ref. 34.

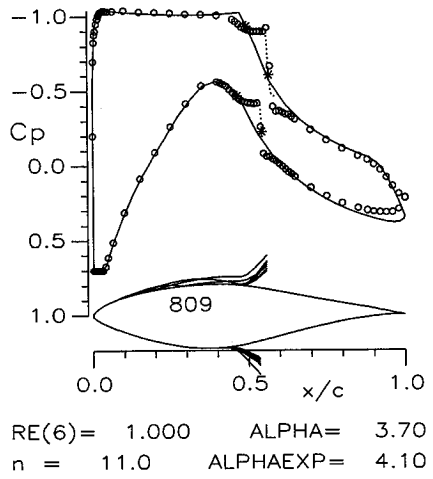

Fig. 8 Comparison of predicted and measured pressure distribution over the S809 airfoil. Solid line: inviscid pressure distribution; dotted line: bubble pressure distribution; circles: data from Ref. 20.

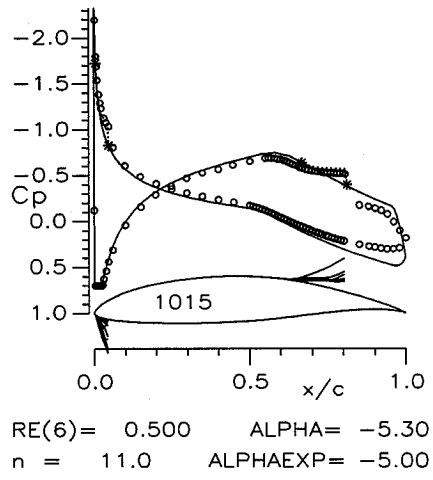

Fig. 9 Comparison of predicted and measured pressure distribution over the NLF(1)-1015 airfoil. Solid line: inviscid pressure distribution; dotted line: bubble pressure distribution; circles: data from Ref. 17.

Pressure Distributions

Figures 8–10 show comparisons of the predicted pressure distributions with the measurements of Refs. 17, 18, and 20 for three different Reynolds numbers. In these figures, neither the inviscid nor the experimental pressure distribution is drawn in the immediate vicinity of the stagnation point. To avoid cluttering the airfoil geometry near the leading edge, the data in this small region are drawn at a constant value of C_p. Figure 8 shows the pressure distribution over the S809 airfoil, designed for a thick wind-turbine blade, at a Reynolds number of 1×10^6. The bubble pressure distributions closely follow the measurements. This figure shows that the transition method employed here[21] is reliable in that it captures the destabilizing effect of the upper surface adverse pressure gradient upstream of the bubble. Figure 9 shows the pressure distribution over the NLF(1)-1015 airfoil at $R = 0.5 \times 10^6$. This case demonstrates that leading-edge bubbles are approximated as accurately as midchord bubbles, as long as the suction peak is not significantly modified by their presence. This airfoil, like the FX 63-137, is strongly aft-loaded and the overall performance prediction using the inviscid distribution is therefore less accurate. Lastly, Fig. 10 shows the pressure distribution over the Eppler E387 airfoil at $R = 1 \times 10^5$. This bubble is quite large, and affects the pressure distribution noticeably over the whole airfoil. The present model driven by the inviscid pressure distribution, however, is still capable of predicting the bubble correctly.

Aerodynamic Characteristics

The remaining figures contain comparisons of predicted drag polars with those obtained experimentally. Figure 11 shows this comparison for the S809 airfoil[20] at $R = 2 \times 10^6$ and 1×10^6. The agreement is excellent. Figure 12 shows the predicted and measured drag polars for the NLF(1)-1015 airfoil at three Reynolds numbers.[17] Here, the agreement is not as good due to the high aft-loading. In particular, $c_{l,\max}$ is overpredicted by the present noninteracting method. Figure 13 shows comparisons for the E387 airfoil at rather lower Reynolds numbers.[18] The excellent agreement also in this regime, where bubbles become almost as long as the airfoil, indicates that the main physical processes have been modeled correctly. A drag polar analysis typically takes 3 min on a

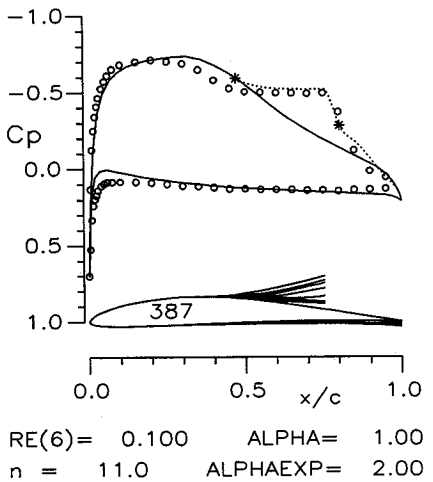

Fig. 10 Comparison of predicted and measured pressure distribution over the E387 airfoil. Solid line: inviscid pressure distribution; dotted line: bubble pressure distribution; circles: data from Ref. 18.

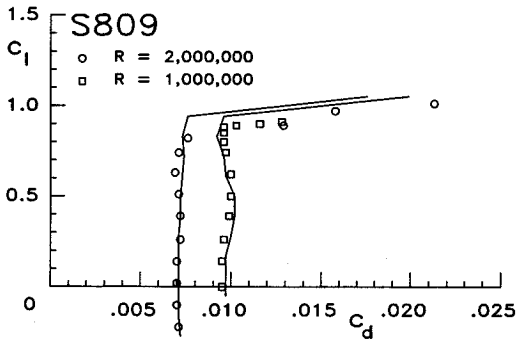

Fig. 11 Comparison of predicted and measured drag polars for the S809 airfoil.[20]

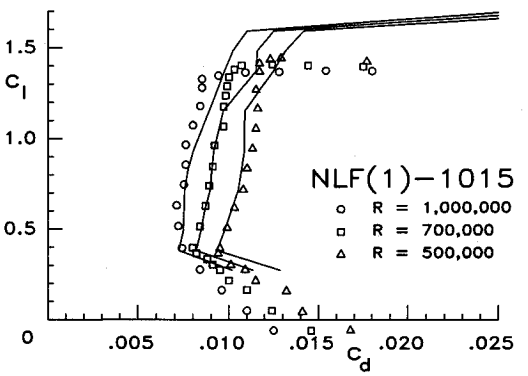

Fig. 12 Comparison of predicted and measured drag polars for the NLF(1)-1015 airfoil.[17]

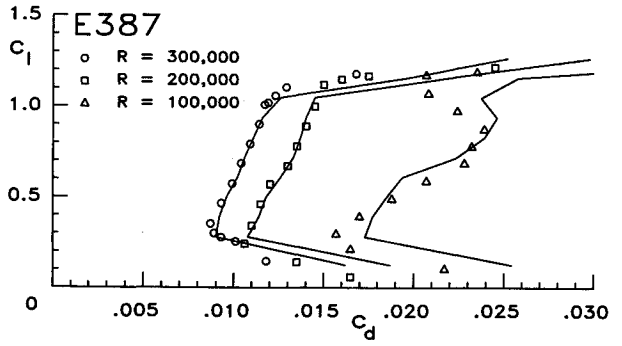

Fig. 13 Comparison of predicted and measured drag polars for the E387 airfoil.[18]

VAXstation 3100, whereas XFOIL[26] takes approximately 30 min on the same machine.

Conclusions

An accurate, general, and efficient laminar separation bubble model has been developed. This model has shown that in the linear range of the c_l curve the weakly interacting boundary-layer model combined with a semi-empirical bubble model gives accurate predictions even at very low Reynolds numbers. The illuminating insights about the physics of this flowfield uncovered during the development of this bubble model, and the improved analysis capability, should benefit the design of improved low-Reynolds number airfoils.

Acknowledgments

The partial support of this work by the NASA Langley Research Center under NASA Grant NAG-1-778 is gratefully acknowledged, as are the valuable inputs from the NASA technical monitor, Dan M. Somers.

References

[1]Jones, B. M., "An Experimental Study of the Stalling of Wings," Aeronautical Research Council, Great Britain, R. & M. 1588, Dec. 1933.

[2]Schmidt, G. S., and Mueller, T. J., "Analysis of Low Reynolds Number Separation Bubbles Using Semiempirical Methods," *AIAA Journal*, Vol. 27, No. 8, 1989, pp. 993–1001.

[3]Drela, M., and Giles, M. B., "Viscous-Inviscid Analysis of Transonic and Low-Reynolds Number Airfoils," *AIAA Journal*, Vol. 25, No. 10, 1987, pp. 1347–1355.

[4]Briley, R. W., and McDonald, H., "Numerical Prediction of Incompressible Separation Bubbles," *Journal of Fluid Mechanics*, Vol. 69, Pt. 4, 1975, pp. 631–656.

[5]Cebeci, T., "Essential Ingredients of a Method for Low Reynolds-Number Airfoils," *AIAA Journal*, Vol. 27, No. 12, 1989, pp. 1680–1688.

[6]Kwon, O. K., and Pletcher, R. H., "Prediction of Incompressible Separated Boundary Layers Including Viscous-Inviscid Interaction," *Journal of Fluids Engineering*, Vol. 101, Dec. 1979, pp. 466–472.

[7]Crimi, P., and Reeves, B. L., "Analysis of Leading-Edge Separation Bubbles on Airfoils," *AIAA Journal*, Vol. 14, No. 11, 1976, pp. 1548–1555.

[8]Davis, R. L., and Carter, J. E., "Analysis of Airfoil Transitional Separation Bubbles," NASA CR-3791, 1984.

[9]Eppler, R., and Somers, D. M., "A Computer Program for the Design and Analysis of Low-Speed Airfoils," NASA TM-80210, 1980.

[10]Eppler, R., *Airfoil Design and Data*, Springer-Verlag, Berlin, 1990.

[11]Dini, P., "A Computationally Efficient Modelling of Laminar Separation Bubbles," Ph.D. Dissertation, Dept. of Aerospace Engineering, Pennsylvania State Univ., University Park, PA, 1990.

[12]Gaster, M., "The Structure and Behaviour of Separation Bubbles," Aeronautical Research Council, Great Britain, R. & M. No. 3595, March 1967.

[13]Wortmann, F. X., "Uber den Ablosewinkel laminarer Ablose-blasen," Deutsche Luft-und Raumfarht Forschungsbericht 74-62 (in German), 1974.

[14]Van Ingen, J. L., and Boermans, L. M. M., "Aerodynamics at Low Reynolds Numbers: A Review of Theoretical and Experimental Research at Delft University of Technology," *International Conference on Aerodynamics at Low Reynolds Numbers* $10^4 < R < 10^6$, Vol. I, Royal Aeronautical Society, London, 1986, pp. 1.1–1.40.

[15]Moran, M. J., "A Unification of Dimensional and Similarity Analysis via Group Theory," Ph.D. Dissertation, Dept. of Mechanical Engineering, Univ. of Wisconsin, Madison, WI, 1967.

[16]Seshadri, R., and Na, T. Y., *Group Invariance in Engineering Boundary Value Problems*, Springer-Verlag, New York, 1985.

[17]Maughmer, M. D., and Somers, D. M., "Design and Experimental Results for a High-Altitude, Long-Endurance Airfoil," *Journal of Aircraft*, Vol. 26, No. 2, 1989, pp. 148–153.

[18]McGhee, R. J., Walker, B. S., and Millard, B. F., "Experimental Results for the Eppler 387 Airfoil at Low Reynolds Numbers in the Langley Low-Turbulence Pressure Tunnel," NASA TM-4062, Oct. 1988.

[19]Somers, D. M., "Design and Experimental Results for the S805 Airfoil," National Renewable Energy Lab. Internal Rept., Golden, CO, Oct. 1988.

[20]Somers, D. M., "Design and Experimental Results for the S809 Airfoil," National Renewable Energy Lab. Internal Rept., Golden, CO, March 1989.

[21]Dini, P., Selig, M. S., and Maughmer, M. D., "Simplified Linear Stability Transition Prediction Method for Separated Boundary Layers," *AIAA Journal*, Vol. 30, No. 8, 1992, pp. 1953–1961.

[22]Eppler, R., "Practical Calculation of Laminar and Turbulent Bled-Off Boundary Layers," NASA TM-75328, 1978 (translated from *Ingenieur Archiv*, Vol. 32, 1963, pp. 221–245).

[23]Stewartson, K., "Further Solutions of the Falkner-Skan Equation," *Proceedings of the Cambridge Philosophical Society*, Cambridge, England, UK, Vol. 50, 1954, pp. 454–465.

[24]Fitzgerald, E. J., and Mueller, T. J., "Measurements in a Separation Bubble on an Airfoil Using Laser Velocimetry," *AIAA Journal*, Vol. 28, No. 4, 1990, pp. 584–592.

[25]Green, J. E., "Two-Dimensional Turbulent Reattachment as a Boundary-Layer Problem," *Separated Flows, AGARD Conference Proceedings No. 4, Part 1*, 1966.

[26]Drela, M., "Improvements in Low Reynolds Number Airfoil Flow Predictions with ISES and XFOIL," Massachussetts Inst. of Technology Computational Fluids Lab. Rept. 91-5, Cambridge, MA, 1991.

[27]Van Ingen, J. L., "On the Calculation of Laminar Separation Bubbles in Two-Dimensional Incompressible Flow," *Flow Separation*, AGARD CP 168, 1975.

[28]Stock, H. W., and Degenhart, E., "A Simplified e^n Method for Transition Prediction in Two-Dimensional, Incompressible Boundary Layers," *Zeitschrift Flugwiss, Weltraumforsch*, Vol. 13, 1989, pp. 16–30.

[29]Gleyzes, C., Cousteix, J., and Bonnet, J. L., "A Calculation Method of Leading Edge Separation Bubbles," *Numerical and Physical Aspects of Aerodynamic Flows II*, Springer-Verlag, New York, 1983.

[30]Swafford, T. W., "Analytical Approximation of Two-Dimensional Separated Turbulent Boundary-Layer Velocity Profiles," *AIAA Journal*, Vol. 21, No. 6, 1983, pp. 923–926.

[31]Birch, S. F., and Eggers, J. M., "A Critical Review of the Experimental Data for Developed Free Turbulent Shear Layers," NASA SP 321, 1973, pp. 943–949.

[32]Horton, H. P., "A Semi-Empirical Theory for the Growth and Bursting of Laminar Separation Bubbles," Aeronautical Research Council, C. P. 1073, UK, June 1967.

[33]Brendel, M., and Mueller, T. J., "Boundary Layer Measurements on an Airfoil at Low Reynolds Numbers," *Journal of Aircraft*, Vol. 25, No. 4, 1988, pp. 612–617.

[34]Pucher, P., and Göhl, R., "Experimental Investigation of Boundary Layer Separation with Heated Thin-Film Sensors," *Journal of Turbomachinery*, Vol. 109, April 1987, pp. 303–309.